東北大学機関リポジトリ
TOUR
Tohoku University Repository

Ballistic-Electron-Emission Microscopy at Epitaxial Metal/Semiconductor Interfaces(STM-BEEM interfaces)

著者	Kanel Hans, von, Meyer Thomas, Sirringhaus Henning, Lee Edwin, Y.
journal or publication title	Science reports of the Research Institutes, Tohoku University. Ser. A, Physics, chemistry and metallurgy
volume	44
number	2
page range	157-163
year	1997-03-31
URL	http://hdl.handle.net/10097/28727

Sci. Rep. RITU A44 (1997) pp. 157-163
No. 2, March 1997

Ballistic-Electron-Emission Microscopy at Epitaxial Metal/Semiconductor Interfaces

Hans von Känel, Thomas Meyer, Henning Sirringhaus,* and Edwin Y. Lee†
Laboratorium für Festkörperphysik, ETH Zürich, CH-8093 Zürich, Switzerland

(Received January 21, 1997)

The invention of ballistic-electron-emission microscopy (BEEM) has made it possible to study hot electron transport across interfaces with a spatial resolution unparalleled before. In order to exploit the limits of the method, we have applied BEEM experiments carried out in UHV and at 77 K to epitaxial $CoSi_2$ films on silicon. $CoSi_2$/Si may be considered as a model system for the metal/semiconductor interface, because its atomic structure can be rather well controlled experimentally and has been well characterized by transmission electron microscopy. This overview contains a discussion of the various processes leading to contrast in BEEM images for $CoSi_2$/Si interfaces. The BEEM current may be affected by (a) the atomic surface structure or surface defects, both of which can change the tunneling distribution, (b) inelastic and elastic scattering processes within the metal films and (c) interface scattering or variations of the Schottky barrier height, resulting from interfacial defects. Scattering processes will be shown to be dominant in the case of $CoSi_2$/Si(111) interfaces, since the Schottky barrier height is not measurably affected by interfacial dislocations and other defects. Here, the ultimate resolution limits of the BEEM technique have been reached, in the sense that individual point defects can be resolved. The $CoSi_2$/Si(100) interface represents a more complicated case, where extended defects lead to significant barrier lowering, whereas interface scattering is obscured by the strong modification of the tunneling distribution by surface reconstructions.

KEYWORDS: BEEM, BEES, CoSi2, Si(100), Si(111)

1. Introduction

The invention of ballistic-electron-emission microscopy (BEEM) by Kaiser and Bell[1] has made it possible to study hot electron transport across buried interfaces with a spatial resolution unmatched before. The technique has been described in detail in a number of excellent review articles[2, 3]. In this brief overview we shall discuss the application of BEEM to $CoSi_2$ grown by molecular beam epitaxy (MBE) on Si(100) and Si(111), as an example for an epitaxial metal/semiconductor interface. One of the main reasons for doing BEEM on this system has been that the structural properties of $CoSi_2$/-Si interfaces were studied intensively in the past, both experimentally and theoretically. For lack of space we shall not be able to give credit to the many researchers involved in these studies. Instead, the description of the structural details will be limited to the absolute minimum required to understand the BEEM results. Usually $CoSi_2$ crystallizes with the cubic CaF_2 structure, with a lattice parameter a_{CoSi_2} which is smaller than a_{Si} by 1.2 %. Contrary to heteroepitaxial systems composed of materials with similar crystal structures, a critical thickness up to which a film can grow defect-free does not exist for $CoSi_2$/Si. Here the defect structure is always related to the presence of interfacial steps.

The $CoSi_2$/Si(111) interface has the so-called type B orientation, where the silicide is rotated by 180 degrees around the surface normal with respect to the silicon substrate. As a result, monolayer and bilayer steps (where 1 monolayer= $a_{Si}/\sqrt{3}$) are associated with partial Shockley dislocations lying in the interfacial plane and having Burgers vectors $\vec{b} = a/6\langle 11\bar{2}\rangle$[4]. In strain-relaxed films these dislocations form a quasi-hexagonal network which can be imaged by STM, since the associated strain fields lead to surface protrusions right above the dislocation lines[5]. Apart from the steps/dislocations $CoSi_2$/Si(111) interfaces are uniform, with all interfacial Co atoms being eight-fold coordinated[6].

For the $CoSi_2$/Si(100) interface the situation is much more complicated. First of all, depending on the details of the growth procedure, more than one epitaxial orientation may occur. The most common ones are $CoSi_2(100)$/Si(100) with $[010]_{CoSi_2} \| [010]_{Si}$ and $CoSi_2(110)$/Si(100) with $[1\bar{1}0]_{CoSi_2} \| [01\bar{1}]_{Si}$[7]. Furthermore, for $CoSi_2(100)$/Si(100) two interface structures have been found to coexist, i.e. a 2×1 reconstructed and an unreconstructed interface[8, 9]. The boundaries between 2×1 and 1×2 reconstructed domains are separated by monolayer steps (here 1 monolayer $= a_{Si}/4$). These steps are now associated with dislocations running along $\langle 011\rangle$ directions, the Burgers vectors of which are of type $\vec{b} = a/4\langle 111\rangle$. The same kinds of dislocations (coupled to interfacial steps) have been found between unreconstructed domains as well as between reconstructed and unreconstructed domains[10].

*present address: University of Cambridge, Department of Physics Cavendish Laboratory, Madingley Road, Cambridge CB3 OHE
†present address: ECE Dept., University of California, Santa Barbara, CA 93106, USA

While from the structural point of view the $CoSi_2$/-Si(111) interface is simpler than the $CoSi_2$/Si(100) interface(s), the opposite is true as far as their electronic structure is concerned. First of all none of the six Si conduction minima projects into the $\bar{\Gamma}$ point of the (111) interface Brillouin zone, whereas for the (100) interface this is of course the case. Ballistic electrons injected from an STM tip at an energy close to the Schottky barrier height Φ_b are therefore less likely to reach the Si conduction band minima at a (111) interface in comparison to a (100) interface, since under conditions relevant to BEEM the tunneling distribution is expected to be strongly focused in the forward direction[2, 3]. The electronic structure of the $CoSi_2$/Si(111) interface contains a further peculiarity, however, in the sense that at energies close to Φ_b there are no states available in the projected $CoSi_2$ band structure which could match the Si conduction band states[11]. According to the band structure calculation such states become available only ~ 0.2 eV above Φ_b. Since the phase space available to electrons in $CoSi_2$ does not grow up to at least 0.6 eV above Φ_b, this theoretical prediction is not expected to be very sensitive to the details of the band structure calculations. Of course these considerations apply only to a perfect epitaxial interface , where the wavevector parallel to the interface, $k_{\|}$, is assumed to be strictly conserved. Any deviations from a perfect interface should therefore affect hot carrier transport very directly. This will be shown below to be indeed the case.

In the following we shall briefly review the most important results obtained by BEEM on $CoSi_2$/Si(100) and $CoSi_2$/Si(111) interfaces. Section 2 starts out with a fragmentary description of the experimental setup. In Section 3 the variation of the Schottky barrier height at interfacial dislocations in $CoSi_2$/Si(100) is discussed. Section 4 deals with the elastic scattering of hot carriers at defects lying at the $CoSi_2$/Si(111) interface. In Section 5 we show that inelastic scattering within the $CoSi_2$ films can be used to map their lateral thickness distribution. Finally, in Section 6 the atomic surface structure is shown to be reflected in the BEEM current, making it possible to study the tunneling distribution by BEEM.

2. Experimental setup

The BEEM experiments were carried out in a home-built UHV STM operated at 77 K. The instrument was especially designed in order to handle the 3 inch Si substrates prepared in a VG V80 MBE system, to which the STM chamber is attached [12]. In order to ensure an ohmic collector contact to the BEEM samples a ~ 20 nm thick $CoSi_2$ film was deposited on the entire backside of the degenerately n or p doped Si substrates. The active junction on the front-side was formed by growing epitaxial $CoSi_2$ films with thicknesses ranging from ~ 2 to 8 nm on a typically 300 nm thick undoped Si buffer layer, using a shadow mask (~ 0.5 cm^2) to define the lateral dimensions of the diode. More details on the sample preparation can be found in Refs. [12–14].

$CoSi_2$/Si(111)	$CoSi_2$(100)/Si(100)	$CoSi_2$(110)/Si(100)
0.66 ± 0.03	0.74 ± 0.04	0.58 ± 0.04

Table 1. Schottky barrier heights in eV of differently oriented $CoSi_2$ interfaces measured by BEEM at 77 K.

3. Schottky barrier height variations at interfacial defects

Spatial variations of the Schottky barrier height on a scale of nanometers has been reported before[15, 16]. These variations were probably due to chemical intermixing at the interface. The scale on which barrier height fluctuations can be measured by BEEM is limited by the so-called *pinch-off effect*, caused by the screening of the potential variation in the semiconductor[17]. The transport of hot carriers across an interface is governed by the true three-dimensional potential profile, whose lateral variations cannot be as abrupt as those of the Schottky barrier Φ_b at the metallurgical interface.

First of all Φ_b has been found to depend on the structure of the epitaxial interface. Table 3 summarizes the observations all applying to defect-free regions and a temperature of 77 K[18].

A similar dependence of the Schottky barrier on the epitaxial orientation of $NiSi_2$/Si(111) was measured in a previous BEEM study[19], confirming earlier results obtained from I-V curves on macroscopic diodes[20]. As pointed out in the Introduction, the $CoSi_2$ exhibits exclusively the type B orientation when grown by MBE on Si(111). By contrast, $CoSi_2$(100) and $CoSi_2$(110) are often found to form simultaneously on Si(100). The presence of differently oriented epitaxial grains is not the only source of structural inhomogeneity, however. We have already mentioned the inevitable presence of dislocations associated with interfacial steps. The question arises therefore to what extent the Schottky barrier height might be affected by such extended linear defects. At $CoSi_2$/Si(111) interfaces dislocations of type $\vec{b} = a/6\,\langle 11\bar{2}\rangle$ do not lead to measurable changes in Φ_b (see also Section 4). The situation is completely different at $CoSi_2$(100)/Si(100) interfaces. Fig. 1 shows a topographic STM image (a) and the corresponding BEEM image, obtained on a 3 nm thick $CoSi_2$ film grown on i-Si/n$^+$-Si(100). The feature of relevance is the soft surface step visible in the left part of the image. It is associated with an interfacial monolayer step and a dislocation with Burgers vector $\vec{b} = a/4\,\langle 111\rangle$ (see Introduction). In the BEEM image of Fig. 1(b) it can be seen that the collector current is increased along the dislocation.

There are other linear structures in the image along which the BEEM current is increased as well. They cannot yet be associated with a known interfacial defect. Some additional features, visible both in the topography and the BEEM image, stem from changes of the surface structure. We shall come back to them in Section 6.

In order to investigate the reason for the inhomogeneities in the collector current, it is necessary to change to the spectroscopy mode of BEEM. Fig. 2 shows two spectra, one of which was acquired right on top of a dislocation similar to that of Fig. 1, and the other one

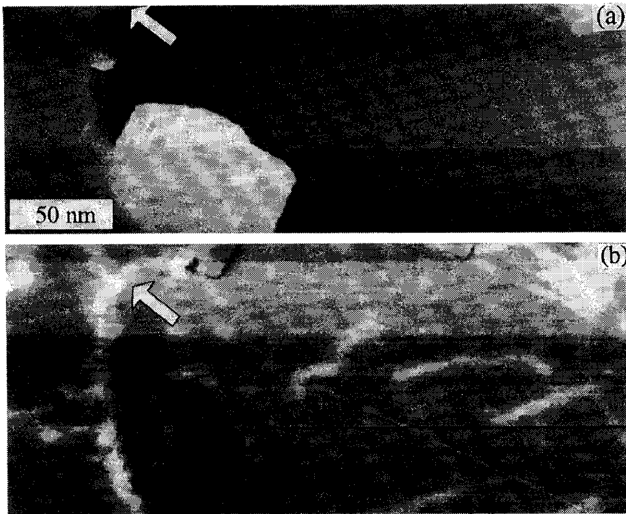

Figure 1. STM topograph (a) and simultaneously acquired BEEM image (b) of a 3 nm $CoSi_2(100)$/n-Si(100) film (V_t=-2 V, I_t=3 nA). The location of a soft surface step is indicated by an arrow. The ranges of the gray scales in (a) and (b) are 0.42 nm and 88 pA, respectively.

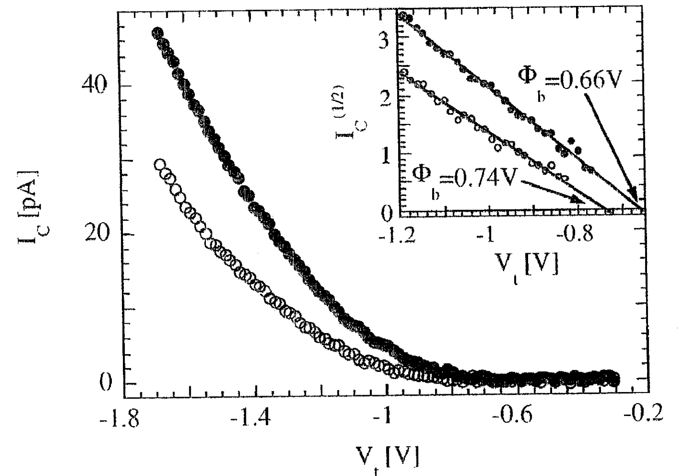

Figure 2. Ballistic-electron-emission-spectra measured next to (open circles) and on top of (filled circles) a a/4(111) dislocation in a $CoSi_2(100)$/n-Si(100) film. In the insert the corresponding thresholds are determined by assuming a square-law behaviour of the BEEM-current close to the onset.

in a defect-free region. The threshold can be seen to be lowered by almost 0.1 eV in the center of the dislocation. We emphasize again that the measured threshold shift, $\delta\Phi_b$, is considerably smaller than the change of the true Schottky barrier height at the metallurgical interface. The latter can be estimated by taking into account the width L of the low-barrier region and the known width of the undoped buffer layer[21]. From spatially resolved spectroscopy along a line perpendicular to the dislocation L can be estimated to be of the order of 4 nm. The calculation shows that the true Schottky barrier practically vanishes within the core of the dislocation.

4. Elastic interface scattering

The $CoSi_2$/n-Si(111) interface is better suited to study hot carrier scattering than $CoSi_2$/Si(100) interfaces. In part this is due to its peculiar electronic structure, already outlined in the Introduction. Furthermore, the surface structure of $CoSi_2$/Si(111) is simpler because it does not exhibit a reconstruction as long as the elastic strain in the silicide is sufficiently relaxed[22]. As a result the contribution of the surface to the BEEM contrast is smaller and interfacial features can be identified more easily (see also Section 6). The $CoSi_2$/Si(111) interface has indeed been the first at which hot electron scattering at interfacial dislocations could be measured by BEEM[23]. An example can be seen in Fig. 3, showing a topographic STM image (a) along with a BEEM image (b). The bright lines in the topographic image are caused by the strain field of interfacial dislocations, leading to a slight deformation of the surface[5]. The dislocations can be seen to show up much more clearly in the BEEM image of Fig. 3(b), where they result in a strong enhancement of the collector current. In addition, the BEEM current is also enhanced at point-like features lying between the dislocation lines. As will be shown below, these features can be explained in terms of hot electron-scattering at interfacial point defects[21]. A closer look at the dislocation contrast shows that most of it is actually also due to point defects, which have been trapped in the strain field of the dislocations. This can be seen in Fig. 4, where line sections taken orthogonal to a dislocation line are plotted. One line shows a pronounced increase of the BEEM current featuring a FWHM of 1 nm due to the presence of a point defect in the core of the dislocation, whereas the BEEM current varies only slowly across a dislocation in the absence of a trapped point defect. In the latter case the BEEM current varies on a scale comparable with the strain field of the dislocation. The extent of the strain field is reflected in the surface corrugation plotted in the topmost curve in Fig. 4.

A further feature noticeable in Fig. 3 is the planar contrast present between different regions bounded by the dislocations. This kind of contrast varies rapidly with the applied tunneling bias. This can be seen in the insert of Fig. 3 in which a BEEM image of the same area, but taken at a different bias, is shown. The planar contrast discussed here vanishes typically above ~2 V. It is caused by a quantum interference effect, leading to standing wave formation in the growth direction (remember that the film thickness changes across each dislocation because of the interfacial step associated with it). The origin of the contrast visible in the BEEM image of Fig. 3 must be due to scattering, since the corresponding spatially resolved spectra reveal a constant threshold of 0.66 ± 0.03 eV, i.e. the Schottky barrier height is not measurably affected by dislocations and point defects at this interface. Since any scattering event taking place at the interface is likely to broaden the momentum distri-

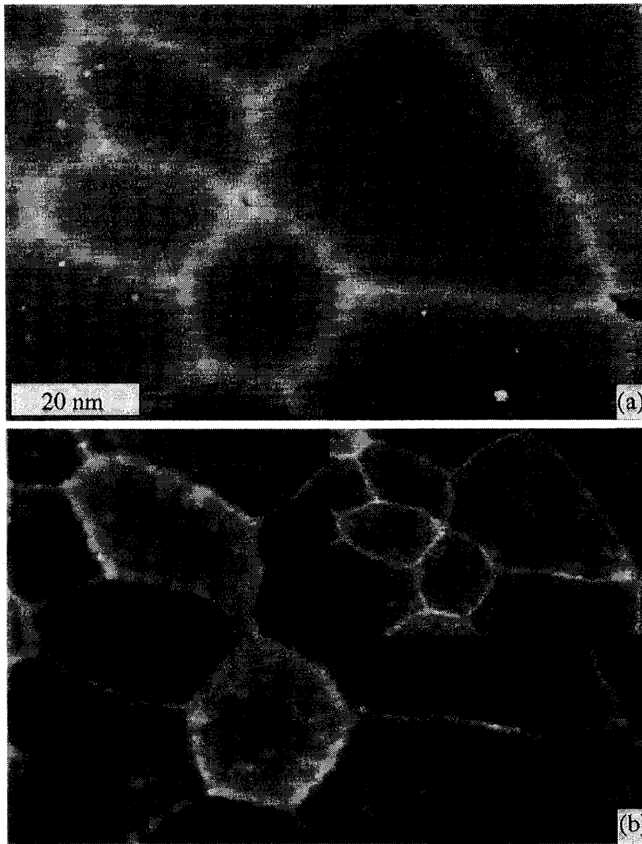

Figure 3. STM topograph (a) and simultaneously acquired BEEM image (b) of a 2.8 nm $CoSi_2$/n-Si(111) film (V_t=-1.2 V, I_t=10 nA). A BEEM image recorded with a tip bias of V_t=-1.6 V is shown in the inset of (b). The ranges of the gray scales in (a), (b) and the inset are 0.21 nm, 277 pA and 507 pA, respectively.

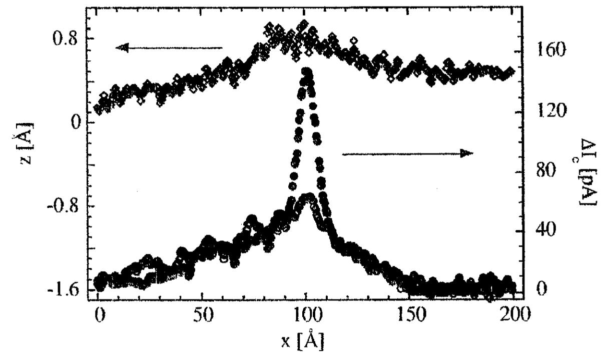

Figure 4. Line sections taken orthogonal to a dislocation line as shown in Fig.3 with (•) and without (○) a point defect present. The current in the line section which does not pass through a point defect shows only a faint variation on a length scale comparable to the surface deformation (◇).

bution, it is reasonable to assume that injection into the off-centered Si conduction band minima will be favoured by such a process. As may be seen in Fig. 3(b) the BEEM current is indeed *enhanced* at every interfacial defect.

The spatial resolution of BEEM contrast caused by scattering is much higher than that due to barrier height variations. Cross-sections through BEEM images such as that of Fig. 3 yield feature sizes as small as 1 nm. The measured halfwidths can vary significantly, however, depending on the condition of the tunneling tip. Since the defects giving rise to contrast variations on such a small scale must be of atomic dimensions, we can obtain a direct measure of the angular distribution of the tunneling electrons from the size of the BEEM features, together with the known film thickness[24]. A simple test for the explanation of the BEEM contrast in Fig. 3 in terms of interfacial scattering can be obtained from the corresponding images taken at $CoSi_2$/p-Si(111) interfaces. It is easy to see that the process of hole injection into the Si valence band is not favoured by interfacial scattering, because of the zone centered valence band maximum. In fact the opposite is true since any scattering event is likely to remove holes from the forward focused tunneling distribution. As a result one should expect the BEEM current to be lowered by the same features leading to its increase in Fig. 3(b). This turns out indeed to be the case as may be seen in Fig. 5 obtained on a 3 nm thick $CoSi_2$/Si(111) film. In the gray-scale representation of Fig. 5(b) all dislocations appear dark, as well as the speckle contrast due to the point defects, which are less well resolved than those in Fig. 3(b). The contrast seen in the BEEM images of Fig. 3(b) and Fig. 5(b) can consistently be explained in terms of hot carrier scattering, or equivalently, by the local violation of $k_{||}$ conservation. If $k_{||}$ was strictly conserved in the defect-free regions, the BEEM current should set in at a higher threshold there, according to band structure calculations[11]. Since this is not observed experimentally, we are forced to postulate the presence of an additional momentum breaking mechanism, such as electron-phonon scattering at the metallurgical interface. It should be mentioned also, however, that a threshold shift of the expected magnitude has been observed in BEEM experiments carried out ex-situ by Kaiser and coworkers[25].

5. Inelastic scattering within the metal film

So far we have been considering hot carriers injected at energies close to the threshold, where ballistic transport is dominant in the absence of elastic scattering. With increasing energy the contrast due to elastic scattering gets weaker and weaker as additional channels for interfacial transmission become operative[23]. In addition, the inelastic mean free path of hot carriers decreases with rising energy, because of the electron-electron interaction becoming more important. This results in a diminishing attenuation length λ of hot carriers as a function of their energy, which is directly accessible by BEEM by measuring the thickness dependence of the collector current at various tunneling voltages[26]. Fig. 6 shows the dependence of λ on the tunneling bias, obtained for $CoSi_2$/n-Si(111). The attenuation length can be seen to decrease from ~ 100 Å close to threshold to about 25 Å at 6 eV. The corresponding values for $CoSi_2$/n-Si(100) have

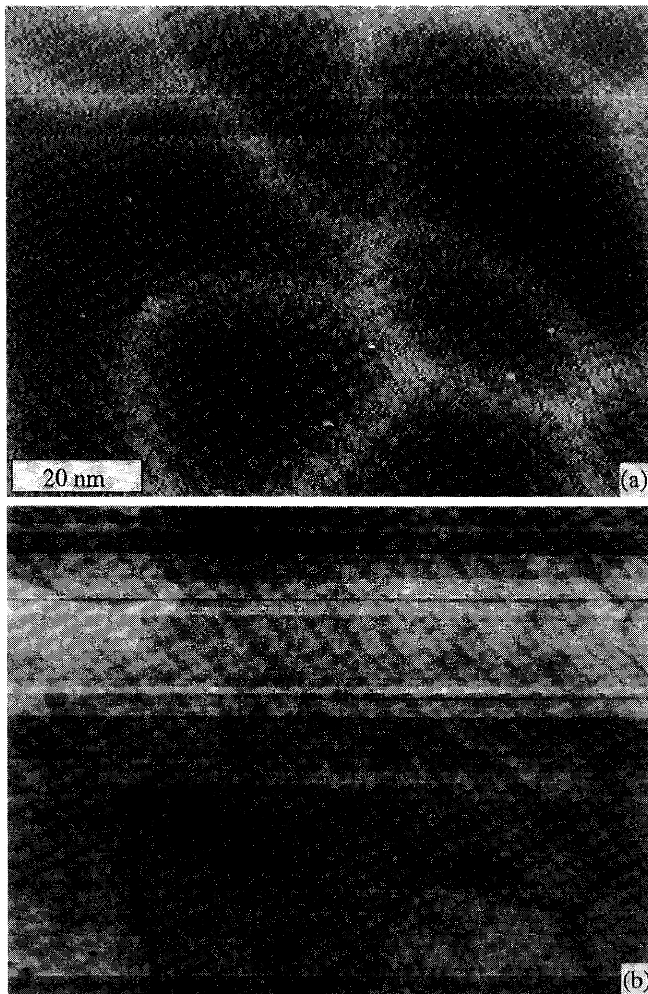

Figure 5. STM topograph (a) and simultaneously acquired BEEM image (b) of a 3 nm $CoSi_2$/p-Si(111) film (V_t=1 V, I_t=20 nA). The ranges of the gray scales in (a) and (b) are 0.22 nm and 360 pA, respectively.

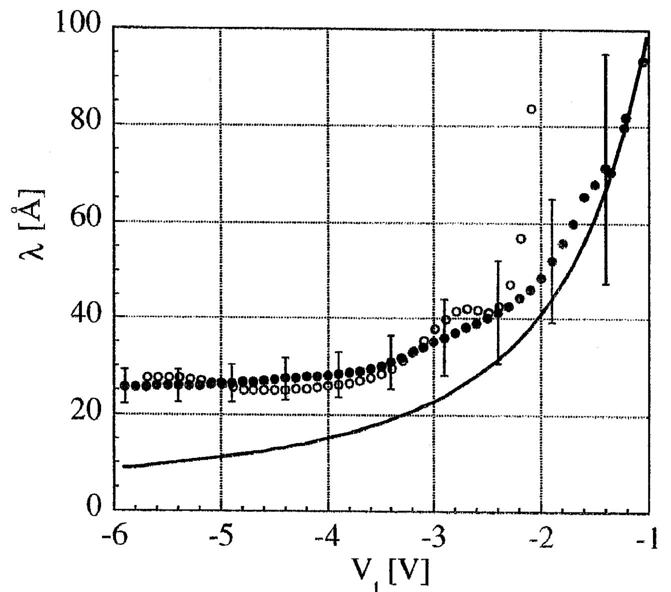

Figure 6. Attenuation length $\lambda(V_t)$ calculated from the thickness dependence of the BEEM current on unreconstructed $CoSi_2$/n-Si(111) (filled circles). Films with film thicknesses of 2.2 nm, 3.0 nm, 4.5 nm, and 7.5 nm were used. The solid curve is a theoretical estimate [27]. The open circles show the values of the attenuation length calculated from contrast observed at a monolayer interfacial step on the 2.2 nm film. They become unreliable below 2.2 V because of the quantum interference effect.

been found to be even shorter[26]. The experimental λ can be seen to saturate at the highest voltages, while the theoretical curve, predicted by a free-electron model continues to decrease (full curve in Fig. 6[27]). This is caused by the generation of secondary electrons in the base, some of which have sufficient energy to surmount the Schottky barrier and thus contribute to the collector current. From a practical point of view the small λ's at high energies provide a convenient way to measure the thickness of the epitaxial silicide films. In fact BEEM images taken at high tunneling biases provide directly real space maps of the film thickness distribution.

An example can be seen in Fig. 7. It has been taken on a 3 nm thick $CoSi_2$/n-Si(111) film at a bias of -6 V. The scanned area contains a number of monolayer surface steps running in a diagonal direction from the upper left to the lower right corners of the topographic STM image (Fig. 7(a)) and the BEEM image (Fig. 7(b)), respectively. As mentioned above, the contrast due to elastic scattering is now entirely absent in the BEEM image. It has been replaced by planar contrast variations corresponding exactly to the areas between the dislocations in the topography image. This is in agreement with the structural studies mentioned in the Introduction[6], according to which the dislocations are associated with interfacial steps. We emphasize that the kind of planar contrast observed here is easily distinguishable from the one caused by the quantum interference effect mentioned in Section 4, since the former varies gradually with the tunneling bias, while the latter shows an oscillatory behaviour.

By comparing cross-sections through BEEM images such as the one of Fig. 7(b) with cross-sections through images obtained at lower energies (e.g. Fig. 3(b)) a considerable degradation of the lateral resolution may be seen[26]. This is again indicative for secondary electron generation within the metal film.

6. Surface effects

The invention of BEEM has clearly been motivated by the wish to have a tool at hand, allowing to measure electric transport across buried interfaces on a small spatial scale. The fact that BEEM is an STM-based technique suggests on the other hand, that the tunneling process itself should play an essential role[2, 3]. The morphology of the surface has long been recognized to affect BEEM imaging to some extent[2, 3]. The observation that even the atomic surface structure may strongly influence the collector current came, however, as a rather unexpected surprise[28, 29]. As an example we display in Fig. 8(a) a topographic image obtained

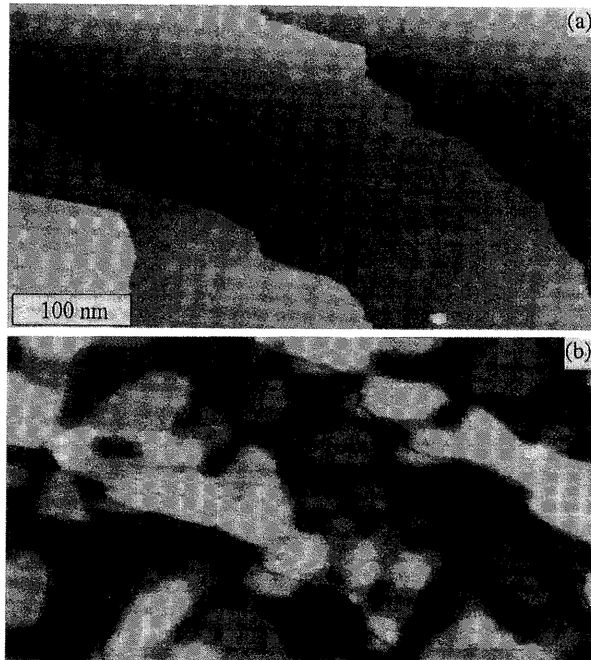

Figure 7. STM topograph (a) and BEEM image (b) taken in the same region of a 2.8 nm $CoSi_2$/n-Si(111) film. Tunneling parameters in (a) and (b) were (V_t=-1.7 V, I_t=3 nA) and (V_t=-6 V, I_t=1 nA), respectively. The ranges of the gray scales are 0.1 nm in (a) and 185 pA in (b).

on a $CoSi_2$(100)/n-Si(100) surface at a higher resolution than the image of Fig. 3(a). In the center part of the image four rows of $3\sqrt{2} \times \sqrt{2}R45^0$ reconstruction running along an $\langle 001 \rangle$ direction can be recognized[14]. In the upper left and lower right corners the surface is $\sqrt{2} \times \sqrt{2}R45^0$ reconstructed instead. As can be seen in the corresponding BEEM image of Fig. 8(b), the collector current exhibits the same spatial periodicity. In particular, the two kinds of reconstructions can be easily distinguished. A closer look reveals, however, that the maxima in the topographic image are associated with *minima* in the BEEM current (see labels in Fig. 8(a) and (b)).

We emphasize that the variation of the BEEM current in Fig. 8(b) is a pure surface effect. Since the tunneling current is kept constant, such a behaviour can only be explained in terms of a variation of the tunneling distribution on a local scale. The interface hence acts as kind of an "analyser", allowing us to see this variation directly. The effect is not restricted to $CoSi_2$(100)/n-Si(100) surfaces. It has been observed in the case of 2×1 reconstructed $CoSi_2$/Si(111) surfaces as well[28], and there are indications that it might be even observable on unreconstructed surfaces under rather extreme tunneling conditions (small tunnel gap).

The transmission of hot carriers across interfaces is sensitive to both the energy as well as the momentum distribution of the tunneling electrons[2, 3]. There are several arguments supporting the conclusion that the en-

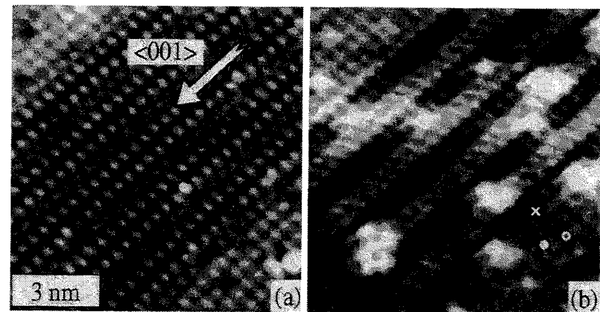

Figure 8. STM topograph (a) and simultaneously recorded BEEM image (b) on the Si-rich $CoSi_2$(100)/n-Si(100) surface (V_t=-1.5 V, I_t=3 nA, film thickness d=3.8 nm). The center part displays a $3\sqrt{2} \times \sqrt{2}$ R45° reconstruction, whereas the lower right and upper left are $\sqrt{2} \times \sqrt{2}R45^0$ reconstructed. The $\sqrt{2}$ topographic corrugation is 0.015 nm. The BEEM contrast ranges from 25 pA (black) to 55 pA (white).

ergy distribution is more important in forming the observed atomic-scale BEEM contrast:

- The reconstruction can be seen in *reverse* BEEM too, where holes are injected from the tunneling tip, while secondary electrons are collected[30].
- The BEEM current is out of phase with the topography at Si(100) and Si(111) interfaces, which would be hard to reconcile with a dominant role of the momentum distribution (see also Section 4).
- Scanning tunneling spectroscopy indicates that the apparent tunneling barrier varies on an atomic scale[28, 29]. The associated variation of the effective tunneling barrier is in qualitative agreement with the BEEM contrast.

7. Summary

We have discussed in this brief overview some of the results obtained by low-temperature UHV BEEM on epitaxial $CoSi_2$/Si interfaces. This model system of a metal/semiconductor interface has turned out to be ideally suited especially for BEEM imaging. Surprisingly large variations of the Schottky barrier height were found to be caused by extended defects at single crystal $CoSi_2$(100)/n-Si(100) interfaces, some of which could be associated with dislocations studied also by transmission electron microscopy. By contrast $CoSi_2$/Si(111) interfaces do not exhibit any measurable barrier height variations. They are, however, very sensitive to all scattering phenomena changing the energy or momentum distribution of injected carriers. Scattering contrast is most pronounced at the $CoSi_2$/n-Si(111) interface, where even single point defects can be identified in BEEM images. The transmission of hot carriers across these epitaxial interfaces is strongly affected by the surface properties of the epitaxial films. This is caused by the influence

of the surface structure on the tunneling distribution, leading to the resolution of surface reconstructions in BEEM images. While this mechanism can be used to study the tunneling distribution, it can also lead to undesirable masking of contrast features stemming from the interface. This is then a further reason for the fact that the best BEEM images have been obtained on unreconstructed surfaces of $CoSi_2$/n-Si(111).

Acknowledgement

Financial support by the Swiss National Science Foundation is gratefully acknowledged.

1) W. J. Kaiser, and L. D. Bell, Phys. Rev. Lett. **60** (1988) 1406
2) M. Prietsch, Physics Reports **253** (1995) 163
3) L.D. Bell and W.J. Kaiser, Annu. Rev. Mater. Sci. **26** (1996) 189
4) R.T. Tung, J.M. Poate, J.M. Gibson, and D.C. Jacobson, Thin Solid Films **50** (1982) 77
5) R. Stalder, H. Sirringhaus, N. Onda, and H. von Känel, Appl. Phys. Lett. **59** (1991) 1960
6) A.F. de Jong and C.W.T. Bulle-Lieuwma, Phil. Mag. (A) **62** (1990) 183
7) S.M. Yalisove, R.T. Tung, and D. Loretto, J. Vac. Sci. Technol. A **7** (1989) 1472
8) D. Loretto, J.M. Gibson, and S.M. Yalisove, Phys. Rev. Lett. **63** (1989) 298
9) C.W.T. Bulle-Lieuwma, A.F. de Jong, and D.E.W. Vandenhoudt, Phil. Mag. A **64** (1991) 255
10) C.W.T. Bulle-Lieuwma, Appl. Surf. Sci. **68** (1993) 1
11) M.D. Stiles and D.R. Hamann, J. Vac. Sci. Technol. B **9** (1991) 2394
12) H. Sirringhaus, E.Y. Lee, and H. von Känel, J. Vac. Sci. Technol. B **12** (1994) 2629
13) H. von Känel, Mat. Sci. Rpts. **8** (1992) 193
14) R. Stalder, C. Schwarz, H. Sirringhaus, and H. von Känel, Surf. Sci. **271** (1992) 355
15) H. Palm, M. Arbes, and M. Schulz, Phys. Rev. Lett. **71** (1993) 2224
16) A.A. Talin, R.S. Williams, B.A. Morgan, K.M. Ring, and K.L. Kavanagh, Phys. Rev. B **49** (1994) 16 474
17) J.L. Freeouf, T.N. Jackson, S.E. Laux, and J.M. Woodall, J. Vac. Sci. Technol. B **21** (1982) 570
18) H. Sirringhaus, E.Y. Lee, and H. von Känel, J. Vac. Sci. Technol. B **13** (1995) 1848
19) A. Fernandez, H.D Hallen, T. Huang, R.A. Buhrman, and J. Silcox, J. Vac. Sci. Technol. B **9** (1991) 590
20) R.T. Tung, Phys. Rev. Lett. **52** (1984) 461
21) H. Sirringhaus, T. Meyer, E.Y. Lee, and H. von Känel, Phys. Rev. B **53** (1996) 15 944
22) R. Stalder, H. Sirringhaus, N. Onda, and H. von Känel, Surf. Sci. **258** (1991) 153
23) H. Sirringhaus, E.Y. Lee, and H. von Känel, Phys. Rev. Lett. **73** (1994) 577
24) H. Sirringhaus, T. Meyer, E.Y. Lee, and H. von Känel, Physica Scripta T**66** (1996) 282
25) W.J. Kaiser, M.H. Hecht, R.W. Fathauer, L.D. Bell, E.Y. Lee, and L.C. Davis, Phys. Rev. B **44** (1991) 6546
26) E.Y. Lee, H. Sirringhaus, U. Kafader, and H. von Känel, Phys. Rev. B **52** (1995) 1816
27) J.J. Quinn, Phys. Rev. **126** (1962) 1453
28) H. Sirringhaus, E.Y. Lee, and H. von Känel, Surf. Sci. **331-333** (1995) 1277
29) H. Sirringhaus, E.Y. Lee, and H. von Känel, Phys. Rev. Lett. **74** (1995) 3999
30) L.D. Bell, M.H. Hecht, W.J. Kaiser, and L.C. Davies, Phys. Rev. Lett. **64** (1990) 2679